

Topological Effects of Noise on Nonlinear Dynamics

Gisela D. Charó,^{1,2,*} Mickaël D. Chekroun,^{3,4} Denisse Sciamarella,⁵ and Michael Ghil^{3,6}

¹*Centro de Investigaciones del Mar y la Atmósfera, Facultad de Ciencias Exactas y Naturales, Universidad de Buenos Aires, C1428EGA CABA, Argentina.*

²*Institut Franco-Argentin d'Études sur le Climat et ses Impacts (IFAECI), UMI 3351 (CNRS-CONICET-UBA), C1428EGA CABA, Argentina.*

³*Department of Atmospheric & Oceanic Sciences, University of California, Los Angeles, CA 90095-1565, USA*

⁴*Weizmann Institute of Science, Rehovot, Israel.*

⁵*Institut Franco-Argentin d'Études sur le Climat et ses Impacts (IFAECI), UMI 3351 (CNRS-CONICET-UBA), C1428EGA CABA, Argentina.*

⁶*Geosciences Department and Laboratoire de Météorologie Dynamique (CNRS and IPSL), École Normale Supérieure and PSL University, 75231 Paris Cedex 05, France*

(Dated: December 22, 2024)

Noise modifies the behavior of chaotic systems. Algebraic topology sheds light on the most fundamental effects involved, as illustrated herein by using the Lorenz (1963) model. This model's deterministic attractor is “strange” but frozen in time. When driven by multiplicative noise, the Lorenz model's random attractor (LORA) evolves in time. Here, we use Branched Manifold Analysis through Homologies (BraMAH) to describe LORA's coarse-grained topology. BraMAH is thus extended from deterministic flows to noise-driven systems. LORA's homology groups differ from the deterministic one and they change in time.

I. INTRODUCTION

The climate system has a complex and nonlinear behavior, and its fundamental components — the atmosphere, oceans, and ice sheets — evolve on many different time and space scales [1, 2]. This unstable and dissipative system exhibits natural variability and is driven by external forcings [3, 4]. Physically open systems, modeled as dynamical systems with time-dependent forcing and coefficients, allow for deterministic as well as random forcing, due to both natural and anthropogenic causes.

The theory of nonautonomous (NDSs; [5]) and random (RDSs; [6]) dynamical systems provides the appropriate mathematical setting to address genuine interaction between intrinsic climate variability and its forced change in time [7]. The climate system's bifurcations [1] have gained further attention since the introduction of the term “tipping points” [8, 9]. The latter generalize, in fact, the bifurcation concept to open systems that are modeled by NDSs or RDSs [3, 4, 10].

In examples such as the ocean's wind-driven circulation [3, 7], a certain degree of realism requires considering not only a stochastic time-dependent forcing but also relying on a model's probability density function (PDF) rather than on pointwise simulation alone. The study of RDSs and their time-dependent invariant measures μ_t , known as sample measures [11, 12], addresses these challenges [7, 13]; see Appendices A–C.

Algebraic topology [14] studies algebraic invariants that classify topological spaces up to homeomorphism [15]. Applications to deterministic dynamical systems

are relatively recent and are also known as chaos topology [16–18]. Chaotic attractors can be classified by their branched manifolds [19, 20].

An approach to extract a branched manifold's topology from time series has been formulated [21] and applied to time series of speech data [22] and to material lines in fluid flows [23]. The approach, called Branched Manifold Analysis through Homologies (BraMAH), uses the latter to extract the topological structure of deterministically chaotic systems from the time series they generate — numerically or experimentally — even in the presence of observational background noise. The procedure requires (a) embedding the time series in a suitable phase space to obtain a multidimensional point cloud, and (b) approximating the structure of the branched manifold that supports the point cloud by a cell complex, as defined in algebraic topology [24]. These cells form a coarse-grained structure or “skeleton” of the branched manifold, whose topology can be algebraically calculated. Some of the branches may have torsions that are important for the correct identification of an attractor; hence BraMAH also distinguishes, for instance, a standard strip from a Möbius strip or a torus from a Klein bottle.

Topological Data Analysis (TDA) relies on recent computational advances, including homology computation from point clouds, to study the shape and structure of large data sets by focusing on the connectivity of the data [25–27]. TDA is used more and more in many research areas that are as diverse as image processing [28], the spread of social and biological contagions on networks [29], percolation theory [30], genomics and evolutionary dynamics [31, 32], protein structure [33], and so on.

Key developments in TDA include the computation of Persistence Homologies (PHs) [34, 35], which use a parameter to construct a family of nested cell complexes

* gisela.charo@cima.fcen.uba.ar

that monitor the “lifetime” of basic topological features in a point cloud, such as its holes. PHs were applied to shed further light on the strange attractor of the Lorenz system [36], among other well-known chaotic systems.

BraMAH [21–23] is a TDA method tailored to study the phase space topology of point clouds generated by deterministic nonlinear dynamical systems. These clouds may represent chaotic attractors, invariant manifolds, and also semi-flows on a broader class of objects that are neither attractors nor manifolds [18]. The specificity of the method concerns the cell complex construction rules, as well as the extraction of the topological properties associated with the complexes so constructed.

The manner in which BraMAH constructs the cell complex differs from other TDA construction methods — such as the Čech or Vietoris-Rips methods — in that it uses the fact that the point cloud under study lies on a branched manifold. This property is used to produce a BraMAH cell complex, i.e. a complex in which each cell represents a large subset of points that jointly approximate a locally Euclidean set, whose dimension respects the local dimension of the branched manifold. The output contains all the information that is needed to identify the organization and connectivity of the branches.

The question that inevitably arises about random attractors is: what is the effect of a stochastic perturbation on a nonlinear system’s topological structure? Chekroun et al. [13] have shown that the well-known smoothing effect of noise disappears in a pullback approach. When the unperturbed nonlinear system’s dynamics is chaotic, the random pullback attractor is a time-dependent object that typically exhibits a fine structure of amazing complexity, which is highlighted by its sample measure.

More precisely, random attractors demonstrate that fractal structures can survive the noise and be fed by it, as shown for the first time numerically in [13] for the stochastic Lorenz [37] model’s random attractor, dubbed LORA. This striking property arises, in particular, when the stochastic-dynamic system’s generator is hypoelliptic and its leading Lyapunov exponent is positive [13].

This paper presents, as far as we know, the first application of BraMAH to nonlinear, chaotic systems driven by noise. In it, we show that the random attractor’s structure is well represented, at each instant in time, by a branched manifold. The latter is defined here locally as an integer-dimensional subset of phase space that provides a robust skeleton of the point cloud associated with the sample measure; see Appendix C. This definition of a branched manifold is more general than the usual one in the purely deterministic context, where the invariant manifold is relative to a flow in phase space and defined through a Birman-Williams projection [17, 19].

The present work shows how the topological structure approximating LORA’s instantaneous sample measure is seen through the lens provided by the homological description of its associated branched manifold. We study here changes in LORA’s topology — *i.e.*, topological tipping points — produced by the driving noise.

II. METHOD

Sciamarella and Mindlin [21, 22] formulated the BraMAH method and used it to extract the topological structure of chaotic flows from time series. To do so, one embeds the time series in a suitable phase space in order to generate a point cloud. Dynamically generated point clouds are well described by a branched manifold. The structure of this invariant manifold can be approximated with “building blocks.”

In algebraic topology, these building blocks are Euclidean closed sets (segments, disks, etc.), called n -cells, where $n \in \mathbb{N}_0$. A point is a 0-cell, a line segment joining two points is a 1-cell, a polygon is a 2-cell and so forth. Constructing and assembling these cells according to the BraMAH rules detailed in Appendix D builds a cell complex that is the branched manifold’s skeleton.

The topological structure of this cell complex is studied by using homology groups [24] and orientability chains [22]. The homology groups H_k identify the k -dimensional holes (k -holes) of a topological space of dimension n , where $k \in \mathbb{N}_0$ and $k \leq n$. The group H_0 identifies the connected components (0-holes), H_1 the cycles (1-holes), H_2 the cavities (2-holes), and if $k \geq 2$, H_k the hypercavities (k -holes). By construction, a BraMAH cell complex is uniformly oriented. The orientability chain indicates the number and location of torsions in the cell complex. For further details of the BraMAH method, see Appendix D.

When evaluating a time-dependent structure like LORA, one has to ask whether its topology is time-dependent. In order to answer this question, we will take two steps: (1) generate the point clouds that approximate LORA at successive time instants, called “snapshots” [13, 38, 39]; and (2) compute the topological properties associated with each snapshot using BraMAH.

In step (1), the point cloud approximating LORA is generated by solutions of the stochastic Lorenz model (SLM) introduced in [13]. In SLM, the equations of the classical Lorenz [37] deterministic model are perturbed by a multiplicative noise in the Itô sense [6], with W_t a Wiener process and $\sigma > 0$ the noise intensity:

$$\begin{aligned} dx &= s(y - x)dt + \sigma x dW_t, \\ dy &= (rx - y - xz)dt + \sigma y dW_t, \\ dz &= (-bz + xy)dt + \sigma z dW_t; \end{aligned} \quad (1)$$

here $r = 28$, $s = 10$, $b = 8/3$ are the standard parameter values for chaotic behavior.

The time-dependent sample measures μ_t associated with the SLM system (1) are probability measures for the population density of any ensemble of initial data driven by the same noise realization until time t , after removal of the transient behavior. Mathematically, these measures are of Sinai-Ruelle-Bowen (SRB) type [12, 40, 41], *i.e.*, they are supported by the foliation of unstable manifolds that structure the random attractor [13].

A numerical estimation $\hat{\mu}_t$ of such a measure can be computed at any time instant t by a pullback ap-

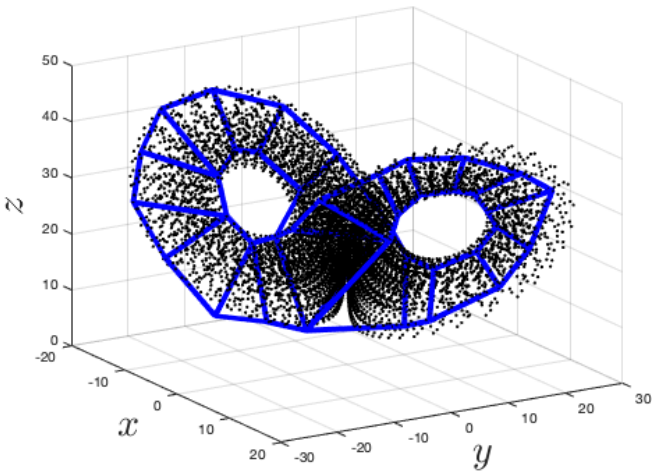


FIG. 1: Point cloud juxtaposed on the cell complex (blue lines) obtained by BraMAH for the deterministic Lorenz [37] attractor, with $\sigma = 0$ in Eq. (1).

proach, *i.e.* by letting a large set of N_0 initial points $\{(x_j, y_j, z_j)(t=0) : j = 1, \dots, N_0\}$ “flow” in phase space from the remote past until time t , for a fixed noise realization ω . The convergence of the sample measure’s approximation $\hat{\mu}_t = \hat{\mu}_t(N_0)$ is studied as the number N_0 of initial points increases; it is observed herein for $N_0 \simeq 10^8$.

Each point within a single point cloud at time t is mapped to a value of $\hat{\mu}_t$ that is obtained by averaging over a volume surrounding that point: higher or lower $\hat{\mu}_t$ -values correspond to more or less populated regions of the random attractor. We are interested in characterizing the topology of the point cloud’s most populated regions but also in ascertaining this topology’s robustness and perdurance as N_0 changes. In order to do this, a threshold \bar{n} for $\hat{\mu}_t$ must be selected, as discussed later.

III. RESULTS

To start our study, we provide first a BraMAH analysis of the classical Lorenz [37] attractor, with $\sigma = 0$ in Eq. (1). The strange attractor and the BraMAH cell complex associated with its branched manifold is shown in Figure 1. The cell complex presents one connected component, *i.e.*, $H_0 \sim \mathbb{Z}$, and two homologically independent 1-holes associated with each wing of the butterfly, *i.e.*, $H_1 \sim \mathbb{Z}^2$; there are no torsions, *i.e.*, $O_1 \sim \emptyset$, and no enclosed cavities, *i.e.*, $H_2 \sim \emptyset$.

Generating point clouds associated with solutions of the SLM yields data sets in the form of 3-dimensional point clouds $\{\mathbf{x}_i \in \mathbb{R}^3 : 1 \leq i \leq N_0\}$ with $N_0 = 10^8$. These point clouds are sieved using a threshold value \bar{n} in the sample measure $\hat{\mu}_t$ in order to keep only those points that correspond to the most populated regions of the cloud. At each \bar{n} value a point cloud $\{\mathbf{x}_i : \hat{\mu}_t(\mathbf{x}_i) \geq \bar{n}\}$ is used to construct one BraMAH cell complex.

At $t = 40.27$, there are only four 1-holes that perdure as the value \bar{n} of the threshold increases. Notice that

such a perdurance plot should not be read as a PH barcode: at each \bar{n} -value, BraMAH uses a point cloud that differs in its size and elements to construct the cell complex, whereas in PHs there is a single point cloud under consideration and the horizontal axis sweeps a parameter value that regulates the construction of nested cell complexes for the same point cloud.

The sieved point cloud used in Figures 2 (b) and (c) is constructed using $\bar{n} = 2 \times 10^{-4}$ as threshold value for the estimated sample measure $\hat{\mu}_t$: Figure 2(b) shows the projection of the sieved point cloud onto the (y, z) -plane, with thirteen 1-holes colored and three of them labeled with the numbers (1), (2) and (3). Panel (c) shows a 3-dimensional view of the sieved point cloud with the perdurant 1-hole labeled with number (4) in red. The colors of the holes correspond to those of the bars in Fig. 2(a). In this work, we analyze the topology of successive LORA snapshots with noise intensity $\sigma = 0.3$.

The local dimension of the branched manifold remains the same as in the deterministic case: LORA is thus a locally 2-branched manifold and no torsions are ever observed, *i.e.*, $O_1 \sim \emptyset$. Noise adds neither connected components nor cavities to the manifold, so that the groups $H_0 \sim \mathbb{Z}$ and $H_2 \sim \emptyset$ are the same as in Figure 1. The topological distinctions between LORA and the classical strange attractor of Lorenz [37] are thus solely present in H_1 . One notices that the number of 1-holes changes from one snapshot to another, with holes created or destroyed by the noise in the course of time.

This situation is illustrated in Figure 3 for three successive snapshots, at $t = 40.09, 40.18$ and 40.27 ; for each snapshot, we selected a threshold value \bar{n} at which the most perdurant 1-holes occur. The sieved point clouds are given in the 3 top panels, while the corresponding cell complexes are presented in the 3 bottom panels. The number of 1-holes undergoes large changes from one snapshot to the next, as suggested by the video of LORA in the Supplementary Material of Chekroun et al. [13].

IV. CONCLUSION

We have presented here a topological analysis of a paradigmatic random attractor associated with the Lorenz convection model. The associated branched manifold provides a coarse-grained skeleton of this attractor.

Our study shows a marked difference between the unperturbed and the noise-driven cases. The stochastically perturbed system’s random attractor, dubbed LORA, presents a much richer structure than the deterministic strange attractor, with a topology that also changes drastically in time. We believe that the framework introduced in this article to characterize such changes in topological features holds promise for the understanding of topological tipping points (TTPs) in general.

A fairly straightforward BraMAH application to the climate sciences might clarify the following quandary of so-called subseasonal-to-seasonal (S2S) prediction [42].

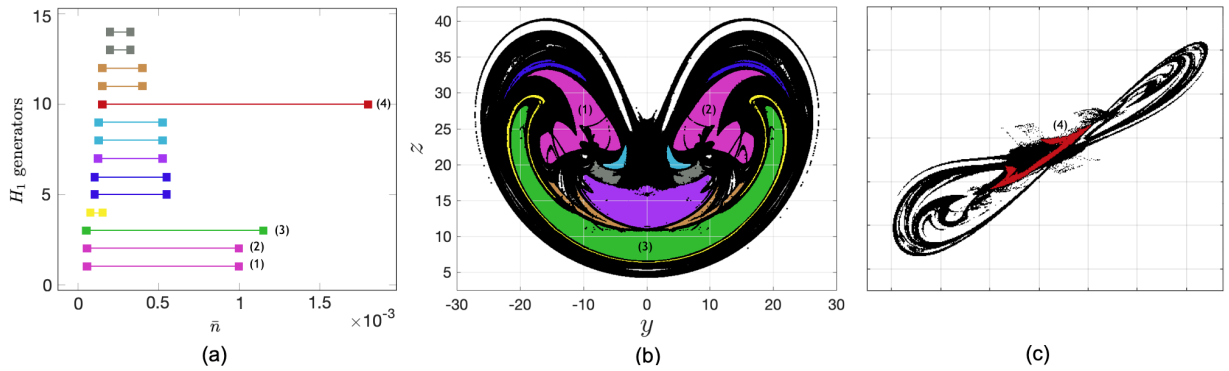


FIG. 2: LORA snapshot at $t = 40.27$, for $\sigma = 0.3$. (a) perdurance of the 1-holes as the density threshold \bar{n} is increased; the most perdurant holes are labeled with numbers (1)–(4); (b) (y, z) projection of the sieved point cloud ($\bar{n} = 2 \times 10^{-4}$) with 13 colored 1-holes; (c) projection onto the plane $-2.25x - 20y + 6z = 0$ of the sieved point cloud with the 1-hole labeled (4) in red.

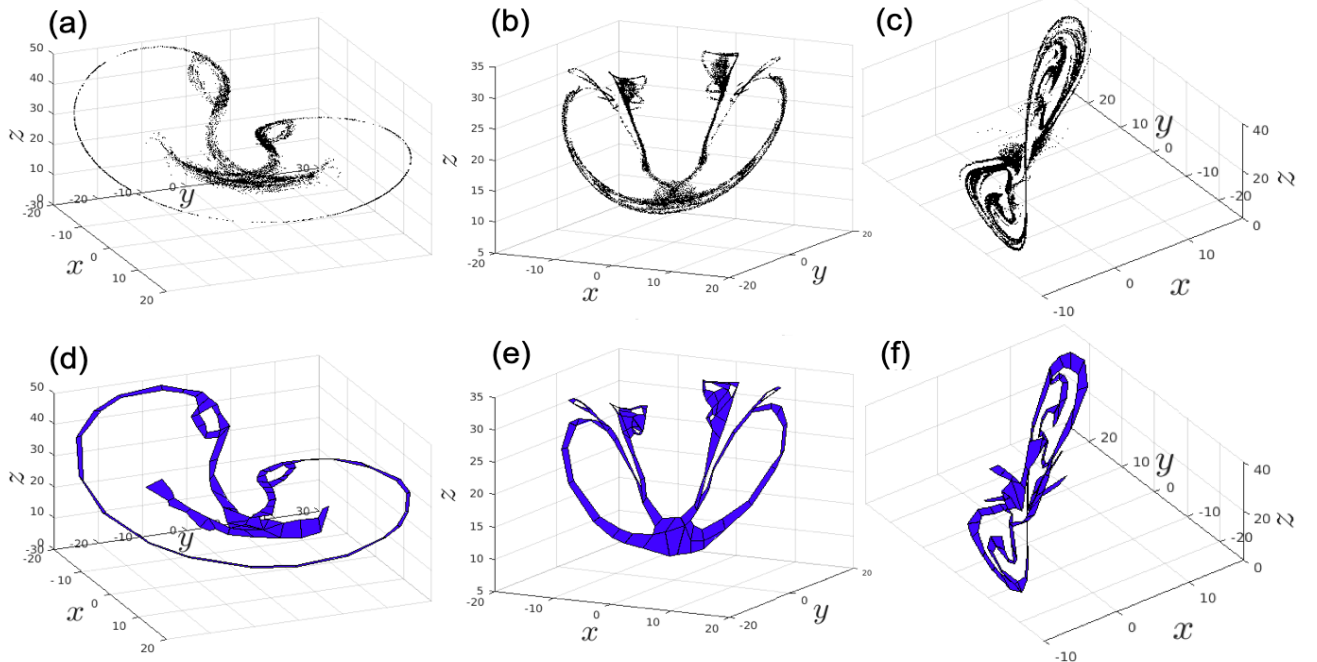


FIG. 3: Two representations of LORA snapshots with $\sigma = 0.3$ and $N_0 = 10^8$: sieved point clouds (a)–(c) and cell complexes (d)–(f). (a,d) $t = 40.09$, $\bar{n} = 6 \times 10^{-4}$, $H_1 \sim \mathbb{Z}^3$; (b,e) $t = 40.18$, $\bar{n} = 2.25 \times 10^{-3}$, $H_1 \sim \mathbb{Z}^{10}$; and (c,f) $t = 40.27$, $\bar{n} = 7 \times 10^{-4}$, $H_1 \sim \mathbb{Z}^4$.

The quandary deals with the role of intermittent vs. oscillatory low-frequency variability (LFV) in the atmosphere [43, 44]. LFV refers to phenomena whose characteristic time of 10–100 days exceeds that of typical mid-latitude storms of 5–7 days [1, Ch. 6].

Such phenomena include the so-called blocking of the westerlies and intraseasonal oscillations with periodicities of 40–50 days; the former is intermittent, or particle-like, the latter oscillatory or wave-like [4, 43]. The quandary is which type of phenomenon dominates LFV and thus could contribute most to S2S prediction [45, Fig. 1].

Blocking has been recently studied in [46] by the unstable periodic orbits methodology of [17]. It would appear that the BraMAH methodology proposed herein could address, more generally and efficiently, the waves-vs.-particles quandary of LFV and how it might be affected by global change [45].

More broadly, tipping points have been given a precise definition in the climate sciences as a generalization to NDSs and RDSs of classical bifurcations in autonomous systems [3, 4, 47] and they are being actively pursued [10, 48–50]. TTPs seem to be a further generalization of the concept that could help us apprehend sudden and drastic changes in time of model behavior, as well as drastic changes due to mean forcing intensity.

The gradual change of atmospheric concentrations of greenhouse gases and aerosols modifies global temperatures in a fairly smooth way [51], as the case has been so far, although it might also lead to dynamical tipping points, as suggested by the above-cited papers. On the other hand, the intrinsic noise associated with cloud processes on small space and time scales affects the entire climate system through their interaction with dynamic and radiative processes on larger scales [e.g., 4, Sec. III.G].

This noise is more complex than the one considered herein and the climate system is infinitely more complex than the Lorenz convection model we have studied. It is quite plausible, and certainly worth exploring further, whether such an interaction between more complex large-scale dynamics and more complex small-scale noise might not lead to striking surprises in not-too-distant times.

ACKNOWLEDGMENTS

This work is supported by the MATH-GEO (18-MATH-04) project of the Regional Program MATH-AmSud (D.S.). G.D.C. gratefully acknowledges support of her postdoctoral scholarship from CONICET and wishes to thank Juan Ruiz and the CIMA computing staff for support with the computations. M.D.C.'s work has been partially supported by the European Research Council (ERC) under the European Union's Horizon 2020 research and innovation program (Grant Agreement No. 810370). The article is TiPES contribution #46; this project has received funding from the European Union's Horizon 2020 research and innovation program under grant agreement No. 820970 (M.G.).

APPENDIX A: PULLBACK ATTRACTORS

We summarize herein some pertinent facts on nonautonomous systems of ordinary differential equations,

$$\dot{x} = F(t, x), \quad t \in \mathbb{R}, \quad (2)$$

considered in the framework of nonautonomous dynamical systems (NDSs); F denotes a smooth time-dependent vector field that governs the time evolution of the state x in a phase space X , taken for simplicity to be the Euclidean space \mathbb{R}^N .

Once existence and uniqueness are guaranteed, one can assign to this NDS a solution map $\Phi(t, s)$, which provides a two-time description of the motion: the time s when the system was initialized, and the time $t \geq s$ of the system's current state. Thus

$$x(t) = \Phi(t, s)x_0$$

denotes the solution of Eq. (2) at time t , when initialized at $x(t) = x_0$ for time $t = s$. In the autonomous case, only the time interval $t' = t - s$ separating s and t matters and $\Phi(t, s)$ reduces to a standard flow $\Phi(t')$.

In the case of forced and dissipative systems, such as the climate system [1, 4], one can define a collection of subsets called a *pullback attractor* (PBA) [6, 7, 10, 13, 52].

Definition 1 *A PBA is a family $\{\mathcal{A}(t)\}_{t \in \mathbb{R}}$, where $\mathcal{A}(t)$ is a compact subset of X at each time t . For each $t \in \mathbb{R}$, this family has two fundamental properties:*

(1) **Invariance:** $\Phi(t, s)\mathcal{A}(s) = \mathcal{A}(t)$, for all $t \geq s$, and

(2) **Pullback attraction:** For any nonempty subset B of X ,

$$\lim_{s \rightarrow -\infty} d_X(\Phi(t, s)B, \mathcal{A}(t)) = 0,$$

where d_X is the Hausdorff semi-distance in X .

According to (1) and (2) above, the family $\mathcal{A}(t)$ is invariant under the system's dynamics and it attracts at each time t all compact initial subsets B from the remote past; see also Ghil et al. [7, Fig. A.1] for a simple illustration.

APPENDIX B: RANDOM DYNAMICAL SYSTEMS (RDS)

In physical systems, such as those encountered in the climate sciences, random time-dependent forcing is often present [4]. When that is so, it becomes necessary to model this type of systems using stochastic differential equations (SDEs) [6].

In the theory of RDSs, random PBAs are known as *random attractors* and they can be constructed in an extended phase space composed of the phase space X and a probability space associated with the paths of the driving noise. A probability space $(\Omega, \mathcal{F}, \mathbb{P})$ is a three-tuple, where Ω is the sample space; \mathcal{F} is the event space, formulated as a σ -algebra; and \mathbb{P} is a probability measure on \mathcal{F} ; see [6, Appendix A].

The probability space is then endowed with a time-dependent shift θ_t . In the case of a stochastic-dynamic system driven by a Wiener process, as is the case here, this shift is defined on Ω according to $W_s(\theta_t \omega) = W_{t+s}(\omega) - W_s(\omega)$ [6]. With this mapping θ_t in hand, the noise realization ω evolves in time, and one can define a cocycle to describe the evolution of the state x .

A mapping $\varphi : \mathbb{R} \times \Omega \times X \rightarrow X$ has the cocycle property when $\varphi(t, \omega) = \varphi(t, \omega, \cdot) : X \rightarrow X$ satisfies the following conditions [6]:

- (i) $\varphi(0, \omega)x = x$, for all $x \in X$ and $\omega \in \Omega$, and
- (ii) $\varphi(t+s, \omega) = \varphi(t, \theta_s(\omega)) \circ \varphi(s, \omega)$, for all $s, t \in \mathbb{R}$ and $\omega \in \Omega$, where \circ denotes the composition operation for mappings of X .

Property (i) just sets the initial state of the cocycle, while property (ii) states that a cocycle is an expression of the existence and uniqueness of solutions, in the sense that going from a copy of X at time 0 to one at time s and from there on to one at time $t+s$ is the same as going directly from 0 to $t+s$; see also Ghil et al. [7, Fig. A.2]. This cocycle property is satisfied for a broad class of SDEs like those of interest here; see [6].

Mathematically, given an SDE with the right properties, the probability space $(\Omega, \mathcal{F}, \mathbb{P})$ equipped with the collections of shifts $\theta = \{\theta_t\}_{t \in \mathbb{R}}$, and its associated cocycle φ , form what is called an RDS (φ, θ) , also called sometimes an RDS φ over θ .

The evolution of a stochastic-dynamic system can thus be modeled by an RDS, while its associated random attractor $\{\mathcal{A}(t;\omega)\}_{t \in \mathbb{R}}$ can be seen as an extension of a PBA, as defined in Appendix A. In the RDS case, however, each individual “random PBA” depends on the specific noise realization ω in Ω . The resulting family $\bigcup_{\omega \in \Omega} \mathcal{A}(t;\omega)$ of random compact sets provides a complete description of all the system’s possible states that are likely to be observed at time t .

APPENDIX C: INVARIANT MEASURES

A number of interesting properties follow from the fact that the RDS (θ, φ) has a random attractor. One of these is the existence of invariant measures of (θ, φ) , in the sense of RDS theory. In this Appendix, we briefly clarify this notion and discuss the properties of these measures.

To do so, recall that any RDS (θ, φ) generates a skew-product semiflow $\{\Theta(t)\}_{t \geq 0}$ on $\Omega \times X$ by the formula

$$\Theta(t)(\omega, x) = (\theta_t \omega, \varphi(t, \omega)x), \quad t \geq 0. \quad (3)$$

The cocycle property for φ is equivalent to the semigroup property for $\Theta(t)$, namely $\Theta(t+s) = \Theta(t)\Theta(s)$. In what follows we denote by \mathcal{B} the σ -algebra of Borel sets in X ; see [6]. We have then the following definition.

Definition 2 *Given an RDS (φ, θ) , a probability measure μ on $(\Omega \times X, \mathcal{F} \times \mathcal{B})$ is called an invariant measure for φ if it satisfies:*

- (i) $\Theta(t)\mu = \mu$, for all $t \in \mathbb{R}$.
- (ii) *The basic probability measure \mathbb{P} is the marginal on (Ω, \mathcal{F}) of μ , i.e. $\mu(E \times X) = \mathbb{P}(E)$ for any $E \in \mathcal{F}$.*

It is known that any probability measure μ on $(\Omega \times X, \mathcal{F} \times \mathcal{B})$ possesses a *disintegration* or factorization [6], given by a function $(\omega, B) \mapsto \mu_\omega(B)$ from $\Omega \times \mathcal{B}$ into the interval $[0, 1]$ such that:

- (i) For any $B \in \mathcal{B}$, μ_ω is \mathcal{F} -measurable;
- (ii) there exists a measurable set Ω' in Ω such that $\mathbb{P}(\Omega') = 1$ and μ_ω is a probability measure on (X, \mathcal{B}) for all ω in Ω' ; and
- (iii) for all f in $L^1_\mu(\Omega \times X)$ we have

$$\int_{\Omega \times X} f(\omega, x) \mu(d\omega, dx) = \int_{\Omega} \left(\int_X f(\omega, x) \mu_\omega(dx) \right) \mathbb{P}(d\omega). \quad (4)$$

The disintegration μ_ω is unique \mathbb{P} -almost surely and it is also called a *sample measure* [41]. The invariance property (i) of Definition 2 translates into $\varphi(t, \omega)\mu_\omega = \mu_{\theta_t \omega}$, in terms of sample measures.

When an RDS (θ, φ) possesses a random compact attractor, then it supports every invariant measure,

i.e. $\mu_\omega(\mathcal{A}(\omega)) = 1$ for almost all ω in Ω . In this case, the sample measure possesses a useful interpretation. To understand it, recall that, roughly speaking, the random attractor $\mathcal{A}(t;\omega)$ determines the portions of the phase space X onto which any bounded set B is mapped at time t , when B is propagated by the cocycle φ from a remote past, for a given noise realization ω . The sample measure $\mu_{\theta_t \omega}$ supported by the random attractor $\mathcal{A}(t;\omega)$ provides, therewith, the spatio-temporal probability distributions of the portions of the phase space X occupied by the RDS, at time t and for the noise realization ω .

For a given stochastic-dynamic system, the set of possible invariant measures is rather large. This raises the question whether a particular class of invariant measures is “naturally chosen” by the dynamics. *Physical measures* are sample measures of special interest in this respect [4, 13]. A probability measure μ is physical if, for any continuous observable $\psi : X \rightarrow \mathbb{R}$, the time average equals the ensemble average for almost all initial data \mathbf{x}_0 that lie in a Lebesgue-positive set B_μ , called the basin of attraction of μ ; see Chekroun et al. [13, Eq. (5)].

Sinai-Ruelle-Bowen (SRB) measures [12, 40, 41] form a closely related class of probability measures. A probability measure μ is an SRB measure if its conditional measures on the unstable manifolds are absolutely continuous with respect to Lebesgue measure. For many dynamical systems, the class of physical measures coincides with that of SRB measures; small differences may exist, however, between the two concepts for certain systems. Regarding the stochastic Lorenz system (1), Chekroun et al. [13, Appendix C] have rigorously shown that LORA supports a random SRB measure when the Kolmogorov operator associated with (1) is hypoelliptic and its leading Lyapunov exponent is positive. Both conditions are met for the parameter values and stochastic forcing used in Eq. (1). Strong numerical evidence provided in [13] suggests that the measure to which the point clouds used herein converge must be physical, too.

Note that the existence of an SRB measure μ does not guarantee its uniqueness, and that two such measures $\mu \neq \nu$ may also have different basins of attraction, $B_\mu \neq B_\nu$. The extensive numerical calculations in [13] and herein have given no indication, though, of such nonuniqueness. Still, the uniqueness of LORA’s random SRB measure or of its physical measure has not been proven rigorously, to the best of the authors’ knowledge.

APPENDIX D: BRAMAH METHOD

BraMAH computes the topology of point clouds whose points are locally distributed on a branched manifold. An m -manifold is a topological space with the property that each point has a neighborhood that is homeomorphic to either a full m -ball or a half m -ball, with $m \in \mathbb{N}$ [18]. In nonlinear dynamics, an m -branched manifold is a mathematical object embedded in a phase space of dimension n ($m \leq n$) that is a manifold everywhere but at the tear

points of the branches [17]. We refer to m as the local dimension of the branched manifold.

Subsets of points of such a point cloud can be locally approximated by m -disks. This decomposition into point subsets or “patches” is called “patch decomposition” [22]. A BraMAH complex is a cell complex constructed so that each patch is associated with a cell in the complex.

To define cell complexes in general, we start with a single cell. A cell of dimension k ($k \in \mathbb{N}_0$) or k -cell is a set that can be mapped through a homeomorphism into the interior of a k -disk, so that the boundaries of the image are divided into a finite number of lower-dimensional cells, called faces. A cell complex \mathbb{K} is a finite set of cells, such that (a) their faces are also elements of the complex; and (b) the interiors of two cells never intersect. \mathbb{K} is said to be an h -complex, or to have dimension h , if its highest dimensional cell is an h -cell.

How does BraMAH construct cells from patches? One first partitions the point cloud $\{\mathbf{x}_i \in \mathbb{R}^n : 1 \leq i \leq N\}$ into overlapping patches that are homeomorphic to the interior of an m -disk. A patch $\{\mathbf{x}_i = (x_{i,1}, x_{i,2}, \dots, x_{i,n}), i = 1, \dots, N_c\}$ is built around a center $\mathbf{x}_0 = (x_{0,1}, x_{0,2}, \dots, x_{0,n})$ by searching for the largest number N_c of points around \mathbf{x}_0 that constitute good approximations to a Euclidean set of dimension m . In order to calculate N_c , candidate sets $\{\mathbf{x}_i, i = 1, \dots, n_c\}$ are computed with its elements sorted by distance from \mathbf{x}_0 , and with $N_{\min} < n_c < N_{\max}$. Given a candidate set, the points \mathbf{x}_i within the ball with center \mathbf{x}_0 and radius r are represented by the neighborhood matrix $X \in \mathbb{R}^{n_c \times n}$:

$$X_{i,j} = \frac{1}{n_c^{1/2}}(x_{i,j} - x_{0,j}).$$

A local coordinate system centered at \mathbf{x}_0 is provided by the singular vectors of X , with the singular values describing the distribution of the points inside the ball centered at \mathbf{x}_0 . For a patch that is approximately lying on an m -disk in \mathbb{R}^n , the local singular spectrum of X has m singular values that scale linearly with n_c as r is increased. This property holds while the effects of the manifold’s curvature are negligible [18, 53]. The remaining $(n - m)$ singular values, which measure the deviation from the tangent space, will scale as r^l with $l \geq 2$.

Using this rule, the m relevant singular values and vectors that span the tangent space approximating the patch under consideration can be identified. The value of N_c is obtained when the m relevant singular values — as functions of n_c subject to $N_{\min} < n_c < N_{\max}$ — exhibit the best linear regression coefficient.

This rule is applied repetitively until every point of the point cloud belongs to at least one patch. The patch axes are chosen so as to favor patch overlapping, in order to keep track of the gluing prescriptions between them. Each patch is transformed into a cell by using convex

hulls, and the singular vectors are used to orient each cell so that neighboring cells have the same orientation, thus resulting in the complex having a uniform orientation. A BraMAH complex is a cell complex that results from applying these steps to an n -dimensional point cloud.

The next step in the BraMAH methodology is to compute the topological properties of the cell complex obtained from the algorithm above. For any given complex, a k -chain is a linear combination of k -cells with integer coefficients. The algebra of these chains allows one to describe the connectivity of the cells at each k -level. A k -hole is a closed chain, called a k -cycle, that is not the border of any higher-dimensional cell.

Our approach uses the labeled list of 0-cells of the BraMAH complex in order to build a boundary matrix and extracts the linearly independent rows of it. Then, it computes the null spaces of the transpose of the boundary matrix and expresses the k -borders in terms of the k -cycles to determine which k -cycles are homologous to others. The k -cycles that are homologically independent are appended to H_k . The integer multiples found in the chain that sums up all the k -borders of the complex are used to form the orientability chain.

The results of this final phase of the method are the homology groups of the BraMAH complex expressed in terms of their generators $\{H_k : k = 0, \dots, h\}$, spelled out in terms of the 0-cells.

The advantages of the BraMAH methodology over PH methods are the following:

- (i) the cell complex’s dimension h agrees with the local dimension m of the branched manifold, which is computed locally using the neighborhood matrix X , and no cells with unnecessarily high dimensions are created;
- (ii) the number of h -cells is significantly lower than the number of points in the original point cloud and the complex they form is thus much easier to study, while other cell complex construction rules produce complexes with numbers of h -cells that vastly outnumber the number of points in the point cloud;
- (iii) the 0-cells of the BraMAH complex are associated with a set of points whose coordinates are identified in the original point cloud; these coordinate values can be used to embed the complex in phase space and to ascertain the mutual organization of the branched manifold’s branches;
- (iv) the k -holes and orientability chains of the complex can be superimposed on the point cloud or, if $n > 3$, on a projection of the point cloud, allowing one to identify the branches, as well as the torsions or twists along them.

-
- [1] M. Ghil and S. Childress, *Topics in Geophysical Fluid Dynamics: Atmospheric Dynamics, Dynamo Theory, and Climate Dynamics* (Springer, 1987, reissued, 2012).
- [2] C.-P. Chang et al., *Climate Change: Multidecadal and Beyond* (World Scientific, 2015).
- [3] M. Ghil, *Earth Space Sci.* **6**, 1007 (2019).
- [4] M. Ghil and V. Lucarini, *Rev. Mod. Phys.* **92**, 035002 (2020).
- [5] P. E. Kloeden and M. Rasmussen, *Nonautonomous Dynamical Systems* (American Mathematical Society, 2011).
- [6] L. Arnold, *Random Dynamical Systems* (Springer, 1988).
- [7] M. Ghil, M. D. Chekroun, and E. Simonnet, *Phys. D* **237**, 2111 (2008).
- [8] M. Gladwell, *The Tipping Point: How Little Things Can Make a Big Difference* (Little, Brown, 2006).
- [9] T. M. Lenton et al., *Proc. Natl. Acad. Sci. USA* **105**, 1786 (2008).
- [10] M. D. Chekroun, M. Ghil, and J. D. Neelin, in *Advances in Nonlinear Geosciences*, edited by A. A. Tsonis (Springer Science & Business Media, 2018), pp. 1–33.
- [11] F. Ledrappier and L.-S. Young, *Probab. Theory Related Fields* **80**, 217 (1988).
- [12] L.-S. Young, *J. Stat. Phys.* **166**, 494 (2017).
- [13] M. D. Chekroun, E. Simonnet, and M. Ghil, *Phys. D* **240**, 1685 (2011).
- [14] H. Poincaré, *J. Éc. polythec. Mat.* **1**, 1 (1985).
- [15] A. Hatcher, *Algebraic Topology* (Cambridge University Press, 2002).
- [16] G. M. Mindlin and R. Gilmore, *Phys. D* **58**, 229 (1992).
- [17] R. Gilmore, *Rev. Mod. Phys.* **4**, 1455 (1998).
- [18] M. R. Muldoon et al., *Phys. D* **65**, 1 (1993).
- [19] J. Birman and R. F. Williams, *Topology* **22**, 47 (1983).
- [20] P. Holmes and R. F. Williams, *Arch. Ratio. Mech. Anal.* **90**, 115 (1985).
- [21] D. Sciamarella and G. B. Mindlin, *Phys. Rev. E* **64**, 036209 (2001).
- [22] D. Sciamarella and G. B. Mindlin, *Phys. Rev. Lett.* **82**, 1450 (1999).
- [23] G. D. Charó, G. Artana, and D. Sciamarella, *Phys. D* **405**, 132371 (2020).
- [24] L. C. Kinsey, *Topology of Surfaces* (Springer, 1997).
- [25] F. Chazal and M. Bertrand, arXiv:1710.04019 (2017).
- [26] L. Wasserman, *Annu. Rev. Stat. Appl.* **5**, 501 (2018).
- [27] J. Murugan and D. Robertson, arXiv:1904.11044 (2019).
- [28] G. Carlsson et al., *Int. J. Comput. Vis.* **76**, 1 (2008).
- [29] D. Taylor et al., *Nat. Commun.* **6**, 1 (2015).
- [30] L. Speidel et al., *Phys. Rev. E* **98**, 012318 (2018).
- [31] J. M. Chan, G. Carlsson, and R. Rabadan, *Proc. Natl. Acad. Sci. USA* **110**, 18566 (2013).
- [32] R. Rabadan and A. Blumberg, *Topological Data Analysis for Genomics and Evolution: Topology in Biology* (Cambridge University Press, 2019).
- [33] M. Gameiro et al., *Jpn J. Ind. Appl. Math.* **32**, 1 (2015).
- [34] H. Edelsbrunner and J. Harer, *Contemp. Math.* **453**, 257 (2008).
- [35] G. Carlsson, *Acta Num.* **23**, 289 (2014).
- [36] S. Maletić, Y. Zhao, and M. Rajković, *Chaos* **26**, 053105 (2016).
- [37] E. N. Lorenz, *J. Atmos. Sci.* **20**, 130 (1963).
- [38] F. J. Romeiras, C. Grebogi, and E. Ott, *Phys. Rev. A* **41**, 784 (1990).
- [39] G. Drótos, T. Bódai, and T. Tél, *J. Climate* **28**, 3275 (2015).
- [40] J.-P. Eckmann and D. Ruelle, *Rev. Mod. Phys.* **57**, 617 (1985).
- [41] L.-S. Young, *J. Stat. Phys.* **108**, 733 (2002).
- [42] A. W. Robertson and F. Vitart, eds., *The Gap Between Weather and Climate Forecasting: Sub-Seasonal to Seasonal Prediction* (Elsevier, 2018).
- [43] M. Ghil and A. W. Robertson, *Proc. Natl. Acad. Sci. USA* **99**, (Suppl. 1), 2493 (2002).
- [44] M. Ghil, A. Groth, D. Kondrashov, and A. W. Robertson, in *The Gap Between Weather and Climate Forecasting: Sub-Seasonal to Seasonal Prediction*, edited by A. W. Robertson and F. Vitart (Elsevier, Amsterdam, The Netherlands, 2018), chap. 6, pp. 119–142.
- [45] M. Ghil, *Nonlinear Process. Geophys.* **27**, 429 (2020).
- [46] V. Lucarini and A. Gritsun, *Clim. Dyn.* **54**, 575 (2020).
- [47] P. Ashwin, S. Wiczorek, R. Vitolo, and P. Cox, *Philos. Trans. R. Soc. A* **370**, 1166 (2012).
- [48] T. Tél, T. Bódai, G. Drótos, T. Haszpra, M. Herein, B. Kaszás, and M. Vincze, *J. Stat. Phys.* **179**, 1496 (2020).
- [49] S. Pierini, M. Ghil, and M. D. Chekroun, *J. Climate* **29**, 4185 (2016).
- [50] S. Pierini, M. D. Chekroun, and M. Ghil, *Nonlinear Process. Geophys.* **25**, 671 (2018).
- [51] IPCC, *Climate Change 2007 - The Physical Science Basis: Working Group I Contribution to the Fourth Assessment Report of the IPCC* (Cambridge University Press, Cambridge, UK and New York, NY, USA, 2007), URL <http://www.worldcat.org/isbn/0521880092>.
- [52] T. Caravallo, G. Łukaszewicz, and J. Real, *Nonlinear Anal.* **64**, 484 (2006).
- [53] D. S. Broomhead, R. Jones, and G. P. King, *J. Phys. A* **20**, L563 (1987).